*Danielle J. Moreau , Zebb Prime and Con J. Doolan

An experimental study of the flow-induced noise created by a wall-mounted finite length airfoil

20th AIAA/CEAS Aeroacoustics Conference, 2014 / pp.2014-3290-1-2014-3290-16

AIAA Aviation
16-20 June 2014, Atlanta, GA
20th AIAA/CEAS Aeroacoustics Conference

An Experimental Study of the Flow-induced Noise Created by a Wall-mounted Finite Length Airfoil

Danielle J. Moreau*, Zebb Prime† and Con J. Doolan‡
The University of Adelaide, South Australia, Australia 5005

This paper presents the results of an experimental investigation of the sound produced by flow interaction with a wall-mounted finite length airfoil at low-to-moderate Reynolds number. Acoustic measurements have been taken in an anechoic wind tunnel at a range of Reynolds numbers, angles of attack and for a variety of airfoil aspect ratios (airfoil length to chord ratio) with a single microphone and two perpendicular planar microphone arrays. For comparison, measurements have also been taken with a semi-infinite or two-dimensional airfoil and a half-span airfoil with tip flow but no boundary layer impingement. The experimental data is used to examine changes in wall-mounted finite airfoil noise production as a function of Reynolds number, angle of attack and airfoil aspect ratio. Additionally, the data gives insight into the airfoil noise generation mechanisms and the influence of flow at the airfoil tip and wall junction on noise production.

I. Introduction

Flow-induced airfoil noise is a common phenomena in many engineering applications and is a much studied topic. The majority of studies on airfoil noise have focused on the sound generated by flow over two-dimensional or semi-infinite airfoils.[1–12] The dominant noise generation mechanism in these studies is trailing edge noise and the sound generated depends on Reynolds number and angle of attack. Turbulent trailing edge noise at high Reynolds number is typically broadband in nature while tonal noise can occur at low-to-moderate Reynolds number ($Re_c < 2 \times 10^6$, based on chord) and is commonly attributed to an aeroacoustic feedback loop between instabilities in the boundary layer and acoustic waves generated at the trailing edge.[3,9–11] In comparison, there have only been two reported studies on the sound generated by flow over wall-mounted finite airfoils.[13,14] This is despite the fact that many real world applications use wall-mounted finite airfoils such as wind turbine blades attached to a hub, submarine hydrofoils mounted to a hull or stators connected to a hub or outer wall.

The flow field around a wall-mounted finite airfoil is complex and features a number of three-dimensional fluid phenomena due to end effects, as shown in Fig. 1. In the lower boundary layer, a horseshoe vortex system is present around the airfoil base and extends into the wake.[15–17] Vortex structures may also form at the tip of the finite airfoil, convect downstream of the airfoil trailing edge and eventually form a trailing vortex.[18] These tip and junction vortex structures may form depending on the airfoil aspect ratio (length to chord ratio L/C) and the airfoil length to thickness ratio, L/T, which influences how much flow goes over the tip of the airfoil instead of around it. Other factors that influence the flow field include the airfoil leading and trailing edge bluntness, Reynolds number, angle of attack, the incoming boundary layer thickness, the free-stream turbulence level and the roughness of the wall and airfoil surface.[19]

Brooks and Marcolini[13] have conducted one of only two reported experimental studies on the sound produced by a wall-mounted finite airfoil in an effort to investigate tip noise generation. In their study, acoustic measurements were taken for a tripped wall-mounted NACA 0012 airfoil with 5 different length to thickness ratios between $L/T = 8.3$ - 50 at Reynolds numbers of up to $Re_c = 1 \times 10^6$, based on chord. Kendall[14] has also measured the noise produced by a tripped wall-mounted NACA 0012 airfoil with $L/T = 19$

*Research Associate, School of Mechanical Engineering, danielle.moreau@adelaide.edu.au, AIAA member
†Research Associate, School of Mechanical Engineering, zebb.prime@adelaide.edu.au, AIAA member
‡Associate Professor, School of Mechanical Engineering, con.doolan@adelaide.edu.au, AIAA Senior member

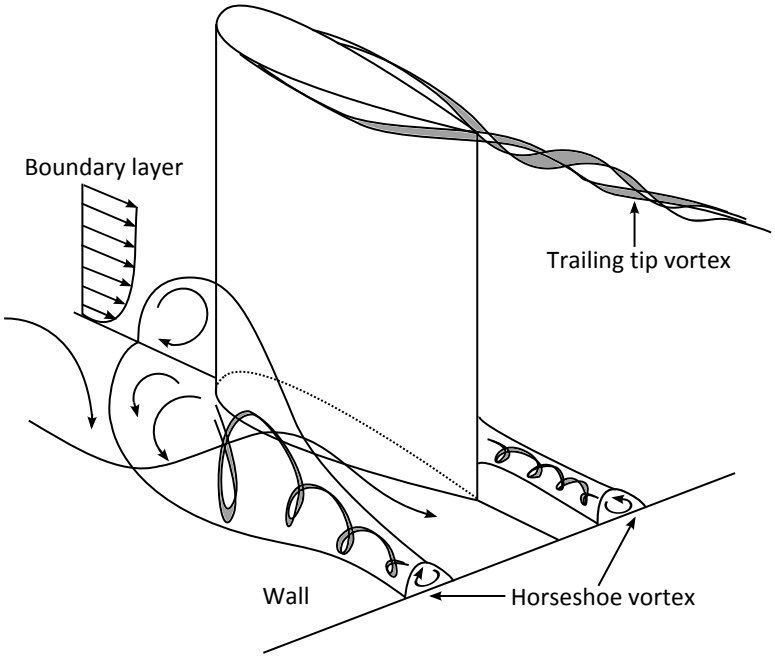

Figure 1: Flow around a wall-mounted finite airfoil.

at a Reynolds number of $Re_c = 2.8 \times 10^5$. Using a directional microphone system, the dominant noise source was found to be located at the corner of the airfoil tip and trailing edge.

This paper presents the results of an original experimental study of the flow-induced noise created by a wall-mounted finite airfoil at low-to-moderate Reynolds number. It presents, for the first time, noise data for a wall-mounted finite airfoil taken at a single observer location and using two perpendicular planar microphone arrays in the anechoic wind tunnel at the University of Adelaide. Acoustic data are presented for a variety of airfoil aspect ratios (length to chord ratio of $L/C = 0.2 - 2$, corresponding to length to thickness ratio of $L/T = 1.7 - 16.7$), Reynolds numbers ($Re_c = 1.0 \times 10^5 - 1.3 \times 10^5$) and angles of attack ($\alpha = 0 - 3.2°$). For comparison, acoustic measurements are also presented for a semi-infinite or two-dimensional airfoil and a half-span airfoil with tip flow but no boundary layer impingement. The overall aims of this paper are: (1) to determine the influence of Reynolds number, airfoil aspect ratio and angle of attack on wall-mounted finite airfoil noise generation and (2) to investigate how flow at the airfoil tip and wall junction affects airfoil noise production.

II. Experimental method

II.A. Test model

The test model consists of a finite length NACA 0012 airfoil with flat ended tip fixed to a side plate, as shown in Fig. 2. The side plate is in turn flush mounted to the contraction so that the airfoil length axis (span) is perpendicular to the direction of the flow. Figure 3 shows the finite airfoil attached to the side plate. The co-ordinate system is also shown in Fig. 3 where x is the streamwise direction, y is the spanwise direction and z is the vertical direction. The origin of the co-ordinate system is located at the centre of the junction between the contraction outlet and the side plate. The aluminum side plate has a length of 300 mm in the streamwise (x) direction and a width of 155 mm in the vertical (z) direction. The leading edge of the airfoil is positioned at 90 mm downstream of the jet exit plane at the vertical centreline of the jet (at $x = 90$ mm, $z = 0$). A total of 10 airfoils are used in this study, each with a chord of $C = 69$ mm and a length, L, between 13.8 mm and 138 mm. The airfoils have an aspect ratio of $L/C = 0.2 - 2$, corresponding to a length to thickness ratio of $L/T = (L/C)/0.12 = 1.7$ - 16.7. In this study, airfoils are classified using their length to thickness ratio in accordance with previous studies on wall-mounted finite airfoils.[19] In all tests, the airfoils are untripped, allowing natural boundary layer transition to occur.

For comparison, measurements have also been taken with a semi-infinite or two-dimensional NACA

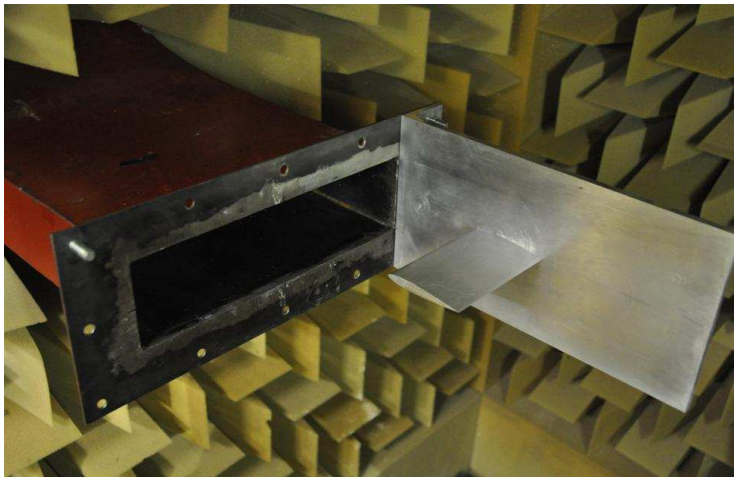

Figure 2: The wall-mounted finite airfoil in the anechoic wind tunnel.

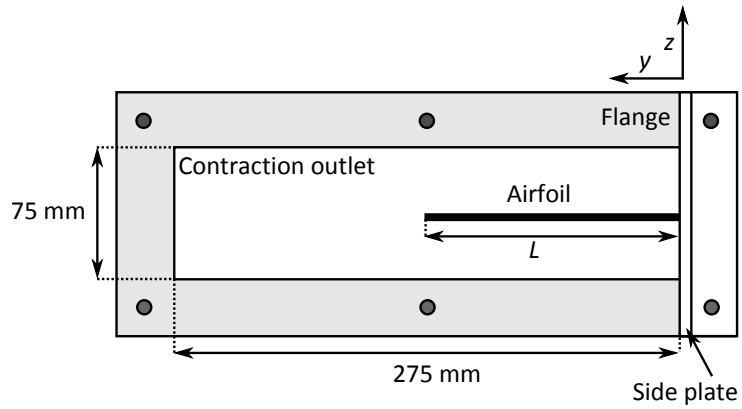

(a) Side view.

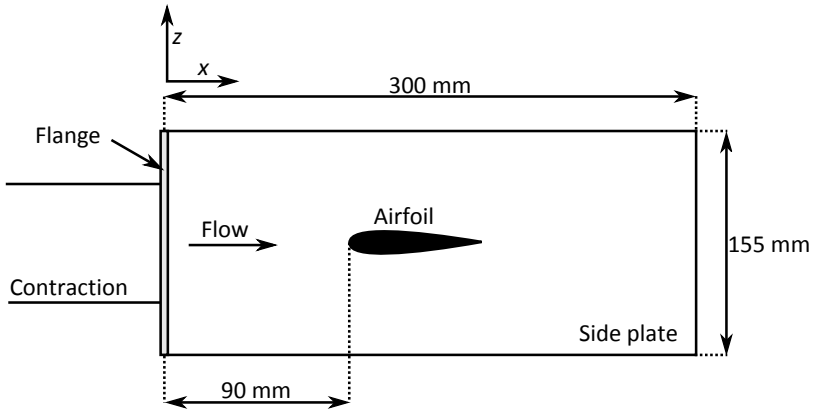

(b) Front view.

Figure 3: Schematic diagram of the wall-mounted finite airfoil attached to the contraction outlet.

0012 airfoil with a chord of $C = 69$ mm and wetted span of $L = 275$ mm, as shown in Fig. 4 (a). This model, referred to as the full-span airfoil, was held using a two sided mounting frame[20] and attached to the contraction with its leading edge positioned at 90 mm downstream of the jet exit plane at the vertical centreline of the jet (at $x = 90$ mm, $z = 0$). The true span of this airfoil model is 450 mm and extends beyond the width of the contraction outlet to avoid a solid wall boundary condition and impinging boundary

layers at the two ends of the airfoil. Additionally, a half-span airfoil with wetted length of $L = 137.5$ mm was attached to one end of the two sided mounting frame, as shown in Fig. 4 (b). This model has a true span of 225 mm and incorporates tip flow effects but does not have the solid wall boundary condition of the wall-mounted finite airfoil. The half-span model is also attached to the contraction with its leading edge positioned at 90 mm downstream of the jet exit plane at the vertical centreline of the jet (at $x = 90$ mm, $z = 0$). The half-span airfoil has a wetted length to thickness ratio of $L/T = 16.6$ which is effectively equivalent to that of the longest wall-mounted finite airfoil with $L/T = 16.7$.

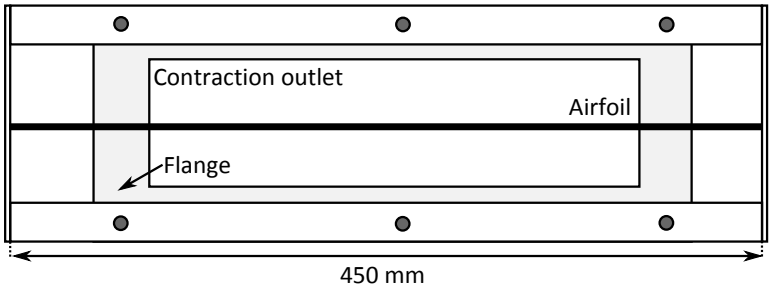

(a) Full-span airfoil.

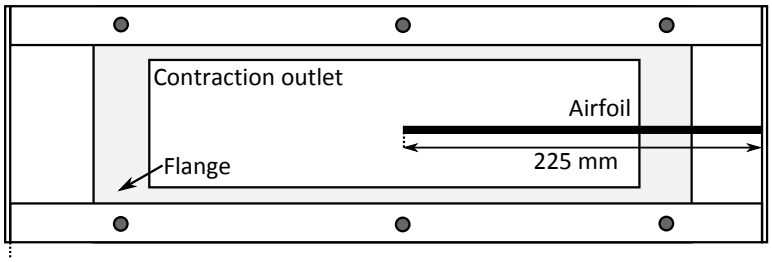

(b) Half-span airfoil.

Figure 4: Schematic diagram of the full-span and half-span airfoil attached to the contraction outlet.

II.B. Anechoic wind tunnel facility

Experiments have been performed in the anechoic wind tunnel at the University of Adelaide. The anechoic wind tunnel test chamber is 1.4 m × 1.4 m × 1.6 m (internal dimensions) and has walls that are acoustically treated with foam wedges providing a near reflection free environment above 250 Hz. The facility contains a contraction outlet that is rectangular in cross-section with dimensions of 75 mm x 275 mm. The maximum flow velocity of the free jet is ~ 40 m/s and the free-stream turbulence intensity at the contraction outlet is 0.33%.[20]

II.C. Measurement techniques

Acoustic measurements have been taken at free-stream velocities of $U_\infty = 20 - 35$ m/s corresponding to Reynolds numbers based on airfoil chord of $Re_c = 9.2 \times 10^4 - 1.6 \times 10^5$. The airfoil models were all tested at geometric angles of attack of $\alpha' = 0°$, 5° and 10° which corresponds to a true angle of attack of $\alpha = 0°$, 1.6° and 3.2° when corrected for the finite height of the contraction outlet.[1]

Acoustic measurements have been recorded at a single observer location using a B&K 4190 1/2" microphone. The microphone was located 500 mm above the (spanwise and chordwise) centre of the wall-mounted finite airfoil with $L/T = 16.7$ (at $x = 124.5$ mm, $y = 69$ mm) for all tests. To provide isolation from wind noise caused by very low level recirculation in the anechoic chamber, a wind sock was placed on the microphone before data collection. Acoustic data have been recorded using a National Instruments PCI-4472 board at a sampling frequency of 5×10^4 Hz for a sample time of 8 s. Data are presented in narrowband format with a frequency resolution of 10 Hz. Spectra have been calculated using Welch's averaged modified periodogram method of spectral estimation with a Hamming window function and 75% overlap.

Two perpendicular planar microphone arrays have also been used to measure the sound emitted by the wall-mounted finite airfoil. Each array consists of 31 GRAS 40PH 1/4" phase matched microphones arranged in Underbrink design[21] in 12 mm MDF board with an EchoSorb 25 (25 mm thickness) sound absorption layer. The first array (termed top array) has a minimum radius of 40 mm, a maximum radius of 490 mm and was located 520 mm above the airfoil surface outside of the flow. The second array (termed side array) has a minimum radius of 40 mm, a maximum radius of 450 mm and was located parallel to the airfoil's tip surface at a distance of 610 mm from the tip of the airfoil with $L/T = 16.7$. Wind socks were placed on all array microphones prior to data collection. The 62 array microphones are connected to a National Instruments PXI-8106 data acquisition system containing 4 PXI-4496 simultaneous sample and hold ADC cards. Data from the 62 microphones were acquired at a sampling frequency of 5×10^4 Hz for a sample time of 10 s. The maps of local sound pressure contributions (or sound maps) presented in this paper have been obtained with the cross-spectral beamforming technique with diagonal removal.[21]

II.D. Side plate boundary layer

To characterize the incoming flow conditions for the wall-mounted finite airfoil, the side plate boundary layer mean velocity profile at the airfoil leading edge location (but with the airfoil removed) has been measured using hot-wire anemometry at $U_\infty = 35$ m/s. A TSI 1210-T1.5 single-wire probe with a wire length of 1.27 mm and a wire diameter of 3.81 μm was used. The sensor was connected to a TSI IFA300 constant temperature anemometer system and positioned using a Dantec automatic traverse with 6.25 μm positional accuracy. The traverse allowed continuous movement in the streamwise (x), spanwise (y) and vertical (z) directions. Velocity data were recorded using a National Instruments PCI-4472 board at a sampling frequency of 5×10^4 Hz for a sample time of 4 s.

The side plate boundary layer mean velocity profile at the airfoil leading edge location at $U_\infty = 35$ m/s is shown in Fig. 5. In this figure, the mean velocity profile is compared with the one-seventh power law for a turbulent boundary layer and the Blasius boundary layer solution for laminar flow. The side plate boundary layer is highly comparable with the one-seventh power law profile, indicating that the flow is well developed and in a turbulent state on the side plate at the airfoil leading edge location. At this location, the boundary layer thickness is $\delta = 10.8$ mm.

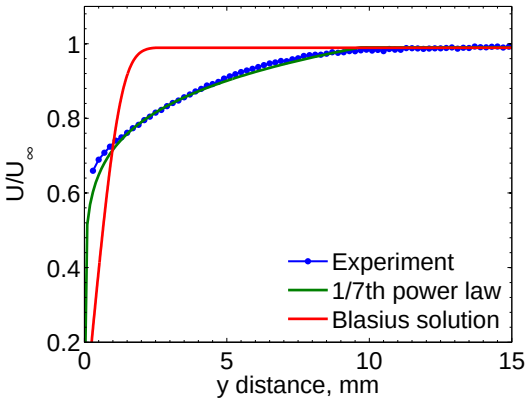

Figure 5: Side plate mean boundary layer profile at the airfoil leading edge location for $U_\infty = 35$ m/s compared to the one-seventh power law profile and the Blasius solution.

The boundary layer thickness has only been measured at $U_\infty = 35$ m/s in this study but it can be approximated at other speeds ($U_\infty = 20 - 30$ m/s) using the expression for a turbulent boundary layer at zero pressure gradient on a flat plate as follows[22]

$$\frac{\delta}{x} = \frac{0.37}{Re_x^{1/5}}, \tag{1}$$

where x is the distance from the origin to the measurement location on the side plate. This distance was calculated using the measured boundary layer thickness at $U_\infty = 35$ m/s in Eq. (1). Table 1 states the flat plate boundary layer thickness at the airfoil leading edge location at flow speeds of $U_\infty = 20 - 35$ m/s and also the ratios of side plate boundary layer thickness to airfoil thickness and length. Table 1 shows that in

this study, the incoming boundary layer thickness to airfoil thickness is $\delta/T = 1.30 - 1.46$. Additionally, the incoming boundary layer thickness is between 7.8% and 88% of the airfoil length.

Table 1: Flat plate boundary layer properties at $U_\infty = 20 - 35$ m/s.

U_∞, m/s	δ, mm	δ/T	$(\delta/L)_{max}$	$(\delta/L)_{min}$
35	10.8	1.30	0.078	0.78
30	11.1	1.34	0.080	0.80
25	11.5	1.39	0.083	0.83
20	12.1	1.46	0.088	0.88

III. Experimental results

III.A. Acoustic spectra

Figures 6 - 8 show single line acoustic spectra for the wall-mounted finite airfoil with $L/T = 8.3$ and 16.7 at flow speeds of $U_\infty = 20 - 35$ m/s and angles of attack of $\alpha = 0 - 3.2°$. Additionally, spectral maps of the noise produced by the wall-mounted finite airfoil with $L/T = 1.7 - 16.7$ at flow speeds of $U_\infty = 20 - 35$ m/s and angles of attack of $\alpha = 0$ and 1.6° are shown in Figs. 9 and 10.

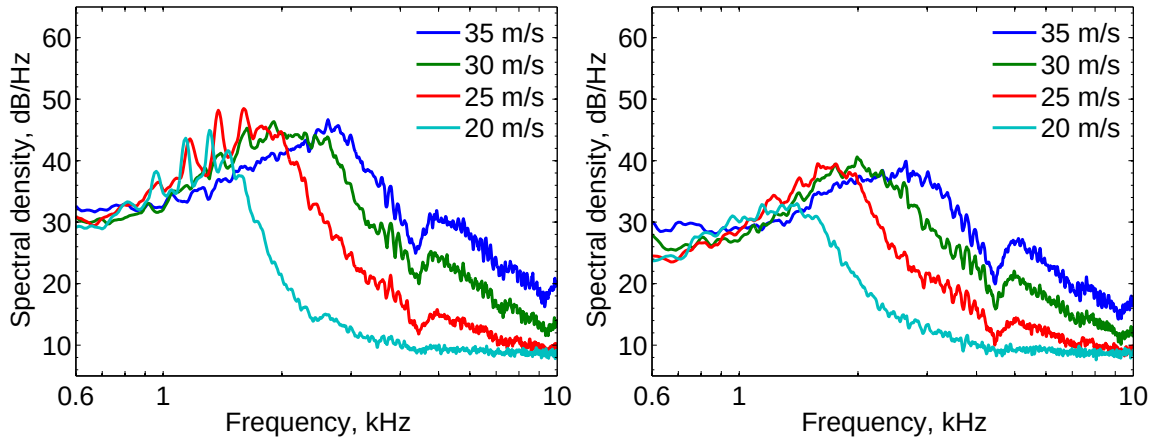

(a) $L/T = 16.7$. (b) $L/T = 8.3$.

Figure 6: Far-field acoustic spectra for the wall-mounted finite airfoil at $U_\infty = 20 - 35$ m/s and $\alpha = 0°$.

At $U_\infty = 35$ m/s and $\alpha = 0°$, Fig. 6 (a) shows the noise radiated by the longest wall-mounted finite airfoil with $L/T = 16.7$ contains high energy at low frequencies and a broad peak centered at a Strouhal number based on airfoil thickness, T, of $St_T = 0.6$. At $U_\infty = 30$ m/s, the noise spectrum of the wall-mounted airfoil with $L/T = 16.7$ displays a broad peak centered at $St_T = 0.6$ and additionally a number of low amplitude peaks also begin to appear. When the flow speed is reduced below $U_\infty = 30$ m/s, these small peaks develop into a number of high amplitude tones. At $U_\infty = 20$ and 25 m/s, the noise radiated by the airfoil with $L/T = 16.7$ consists of a broadband contribution and a number of discrete equispaced tones. At both flow speeds, the value of the difference between two consecutive discrete tonal frequencies is $St_T = 0.05$.

When the angle of attack is increased to $\alpha = 1.6°$, Fig. 7 (a) shows that the longest wall-mounted finite airfoil with $L/T = 16.7$ produces acoustic tones at the higher flow speeds of $U_\infty = 30$ and 35 m/s. At these flow speeds, the spectra display a broadband contribution and a number of discrete tones equispaced by a Strouhal number of $St_T = 0.1$. At lower flow speeds of $U_\infty = 20$ and 25 m/s, the noise radiated by the longest wall-mounted finite airfoil consists of broad peak centered at $St_T = 0.6$.

Figures 6 (b) and 7 (b) show that at $\alpha = 0$ and 1.6°, no tones are produced by the shorter wall-mounted finite airfoil with $L/T = 8.3$. At both angles of attack and all flow speeds between $U_\infty = 20$ and 35 m/s, the spectra for the shorter wall-mounted airfoil display only a broad peak at a Strouhal number of $St_T = 0.6$.

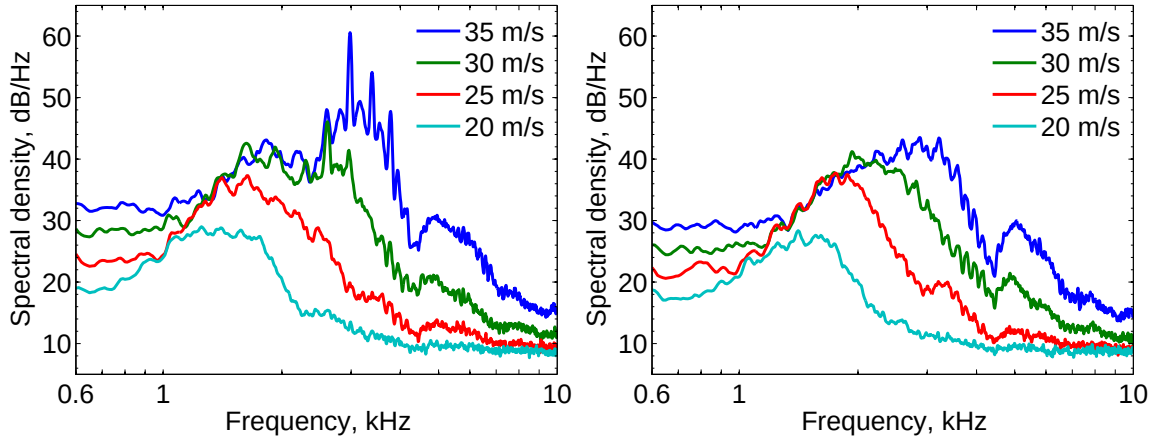

(a) $L/T = 16.7$. (b) $L/T = 8.3$.

Figure 7: Far-field acoustic spectra for the wall-mounted finite airfoil at $U_\infty = 20 - 35$ m/s and $\alpha = 1.6°$.

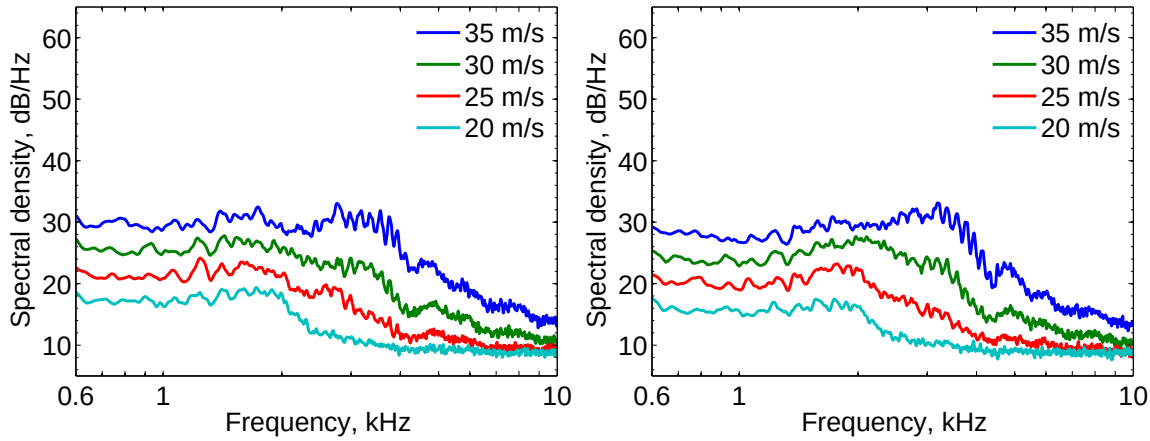

(a) $L/T = 16.7$. (b) $L/T = 8.3$.

Figure 8: Far-field acoustic spectra for the wall-mounted finite airfoil at $U_\infty = 20 - 35$ m/s and $\alpha = 3.2°$.

The spectral maps in Figs. 9 and 10 show that at $\alpha = 0$ and 1.6°, high amplitude acoustic tones are produced by airfoils with $L/T = 10$ - 16.7. Reducing the airfoil aspect ratio has the effect of reducing the noise levels across the entire frequency range of interest. No peaks are observed in the noise spectra for airfoils with $L/T = 1.7$ - 8.3. In this case, it is likely that flow over the tip and at the airfoil-wall junction has suppressed acoustic tone generation. The airfoil length to thickness ratio must therefore be equal to or below $L/T = 8.3$ to produce low amplitude, broadband noise.

At a higher angle of attack of $\alpha = 3.2°$, Fig. 8 shows the noise radiated by the wall-mounted finite airfoil is broadband in nature at all flow speeds and for all airfoil aspect ratios. At this angle of attack, reducing the flow speed and airfoil aspect ratio has the effect of reducing the noise levels across the entire frequency range of interest.

Figure 11 shows the frequencies of the peak tones radiated by the wall-mounted finite airfoil with $L/T = 10 - 16.7$ at $\alpha = 0$ and 1.6°. This figure shows that reducing the airfoil aspect ratio has no effect on the peak tonal frequency when $L/T > 8.3$. The frequencies of the tones increase with an increase in flow velocity and display a ladder type frequency structure consistent with previous studies on two-dimensional airfoil tonal noise at low-to-moderate Reynolds number.[3,23] Paterson et al.[23] found that the frequencies of the tones radiated by a two-dimensional airfoil displayed a dependence on the $U_\infty^{0.8}$ power law and that the frequency scaling law of $U_\infty^{1.5}$ described the relationship between the average behavior of the tonal noise and the free-

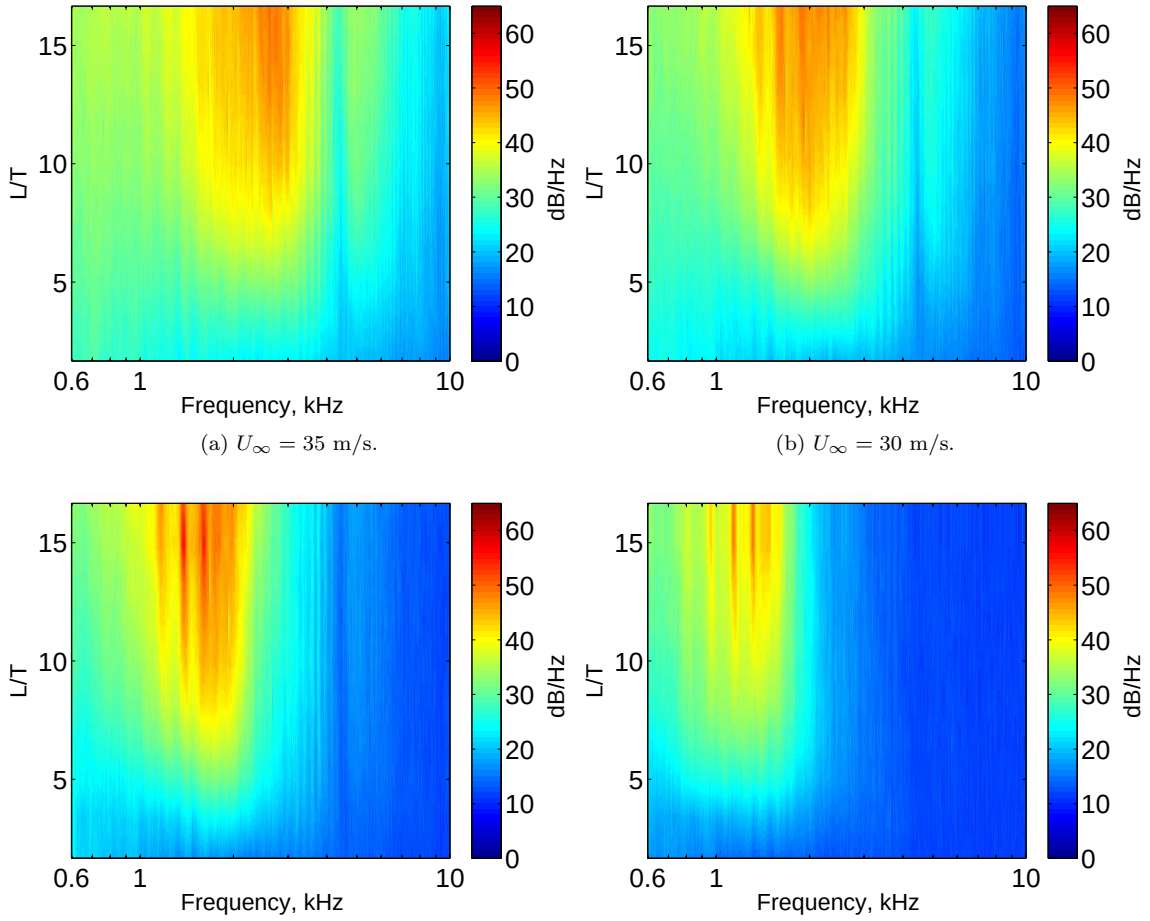

(a) $U_\infty = 35$ m/s.

(b) $U_\infty = 30$ m/s.

(c) $U_\infty = 25$ m/s.

(d) $U_\infty = 20$ m/s.

Figure 9: Acoustic spectral maps for the wall-mounted finite airfoil at $\alpha = 0°$.

stream velocity. These scaling laws do describe the ladder structure of the wall-mounted finite airfoil tonal noise frequencies in Fig. 11 indicating the same noise generation mechanism is responsible for the tonal noise radiated by the wall-mounted finite airfoil. The ladder-type tonal frequency structure of Fig. 11 is commonly attributed to an aeroacoustic feedback mechanism involving convected disturbances in the boundary layer and acoustic waves produced at the trailing edge.[3,9,10]

Lowson et al.[24] developed a tonal envelope that defines the angles of attack and Reynolds numbers for which tones are expected to occur due to an aeroacoustic feedback mechanism. This tonal envelope was derived from experimental data sets for two-dimensional NACA 0012 airfoils.[1,23] Figure 12 shows the operating conditions for which tones are produced by the wall-mounted finite airfoil with $L/T = 10-16.7$ fall within the predicted tonal envelope. The acoustic measurements therefore show that tonal noise generation is occurring presumably in the same manner as in other studies on two-dimensional airfoils, given the similarity of the results to those of others.[23,24]

III.B. Comparison with the full-span and half-span airfoil

Figure 13 shows single line acoustic spectra for the longest wall-mounted finite airfoil with $L/T = 16.7$ compared to that of the full-span and half-span airfoil at flow speeds of $U_\infty = 25$ and 35 m/s and angles of attack of $\alpha = 0 - 3.2°$. As expected the highest noise levels are produced by the full-span airfoil with the largest wetted span and no impinging boundary layer or tip flow. The noise spectra of the half-span airfoil have the same spectral content as that of the full-span airfoil but are reduced in level by up to 3 dB.

At $U_\infty = 35$ m/s and $\alpha = 0°$, Fig. 13 (a) shows tones are produced by the full-span airfoil and additionally,

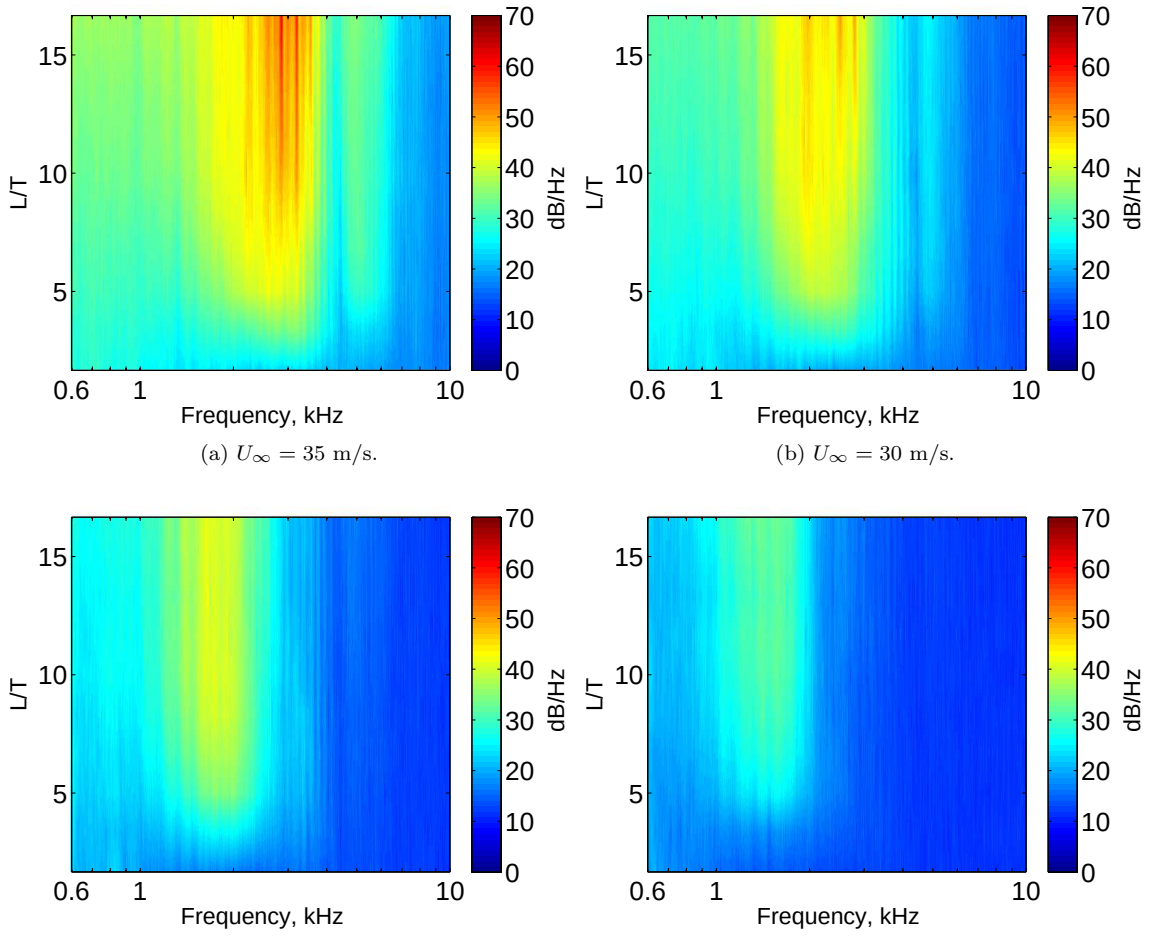

(a) $U_\infty = 35$ m/s.

(b) $U_\infty = 30$ m/s.

(c) $U_\infty = 25$ m/s.

(d) $U_\infty = 20$ m/s.

Figure 10: Acoustic spectral maps for the wall-mounted finite airfoil at $\alpha = 1.6°$.

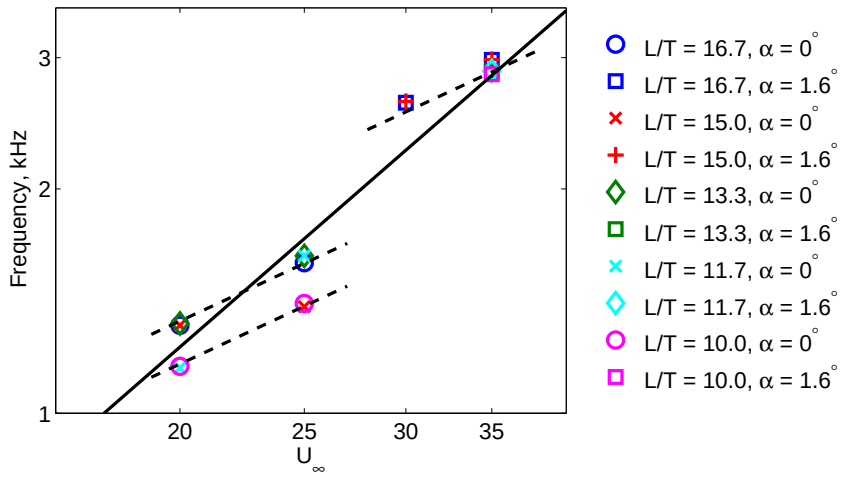

Figure 11: Peak tones radiated by the wall-mounted finite airfoil with $L/T = 10.0 - 16.7$ at $U_\infty = 20 - 35$ m/s and $\alpha = 0$ and 1.6°. Dashed lines represent the power law of $f \sim U^{0.8}$ and the solid line represents the average tonal behaviour of $f \sim U^{1.5}$.

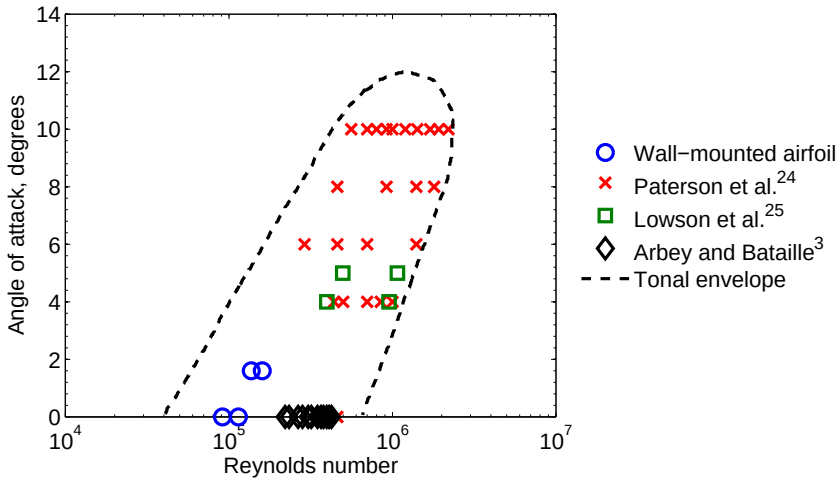

Figure 12: Tonal envelope predicting the operating conditions for tonal noise production from a NACA 0012 airfoil. The measured tones of the wall-mounted finite airfoil with $L/T = 10.0 - 16.7$ at $U_\infty = 20 - 35$ m/s and $\alpha = 0$ and 1.6°are shown along with those measured for a two-dimensional airfoil.[3, 23, 24]

low amplitude peaks are visible in the noise spectrum of the half-span airfoil. In comparison, no tones are produced by the wall-mounted finite airfoil which has the same effective wetted span as the half-span airfoil. This indicates that the combination of junction and tip flow has suppressed tonal noise production in this case. While the overall spectral levels of the half-span and wall-mounted finite airfoil are similar above 1 kHz, the half-span airfoil displays higher noise levels below this frequency and this may be due to shear layer interaction with the end of the half-span airfoil that extends beyond the edge of contraction outlet.

When the flow speed is reduced to $U_\infty = 25$ m/s, Fig. 13 (b) shows tones are produced by the full-span, half-span and wall-mounted finite airfoil at the same frequencies which suggests that the same noise generation mechanism is responsible for tonal noise production from the two- and three-dimensional airfoils. The tones of the wall-mounted finite airfoil are lower in amplitude than those of the half-span airfoil indicating that the introduction of junction flow with tip flow has weakened tonal noise production but not suppressed it in this case. Similar results are observed at $U_\infty = 35$ m/s and $\alpha = 1.6°$ in Fig. 13 (c) which shows that high amplitude tones are produced by the full-span, half-span and wall-mounted finite airfoil. When the angle of attack is increased to $\alpha = 3.2°$, broadband noise is produced by all three airfoils (see Fig. 13 (d)).

III.C. Beamforming results

Figures 14 -17 show sound maps taken with the two perpendicular planar microphone arrays for the wall-mounted finite airfoil with $L/T = 8.3$ and 16.7 at flow speeds of $U_\infty = 25$ and 35 m/s and angles of attack of $\alpha = 0$ - 3.2°.

Figure 14 shows sound maps taken with the top microphone array for the wall-mounted finite airfoil with $L/T = 16.7$ at flow speeds of $U_\infty = 25$ and 35 m/s and zero angle of attack. The locations of the contraction outlet, side plate and airfoil are shown in these figures in white. Sound maps are presented at frequencies from 1 kHz to 7 kHz. At both speeds, the noise source at a frequency of 1 kHz is centered on the airfoil top surface indicating that the airfoil is radiating as a compact source. At higher frequencies of 2 kHz and above, the noise source is located at the trailing edge. At $U_\infty = 25$ m/s, the noise source is reasonably evenly distributed along the airfoil trailing edge from junction to tip while at the higher flow speed of $U_\infty = 35$ m/s, the noise source is shifted closer to the airfoil's free end region and extends from its midspan to tip, agreeing with the early work of Kendall.[14]

For the lower aspect ratio wall-mounted finite airfoil with $L/T = 8.3$, the dominant noise source location is independent of flow speed at all frequencies (see Fig. 15). As observed for the airfoil with $L/T = 16.7$, the noise source at a frequency of 1 kHz is compact while at higher frequencies of 2 kHz and above, the trailing edge is the noise source location. In this case however, the trailing edge noise source at frequencies of 2 kHz and above is distributed along the airfoil span from junction to tip at both flow speeds. At low aspect ratio, the noise source location is insensitive to flow speed suggesting that junction and tip flow have combined to

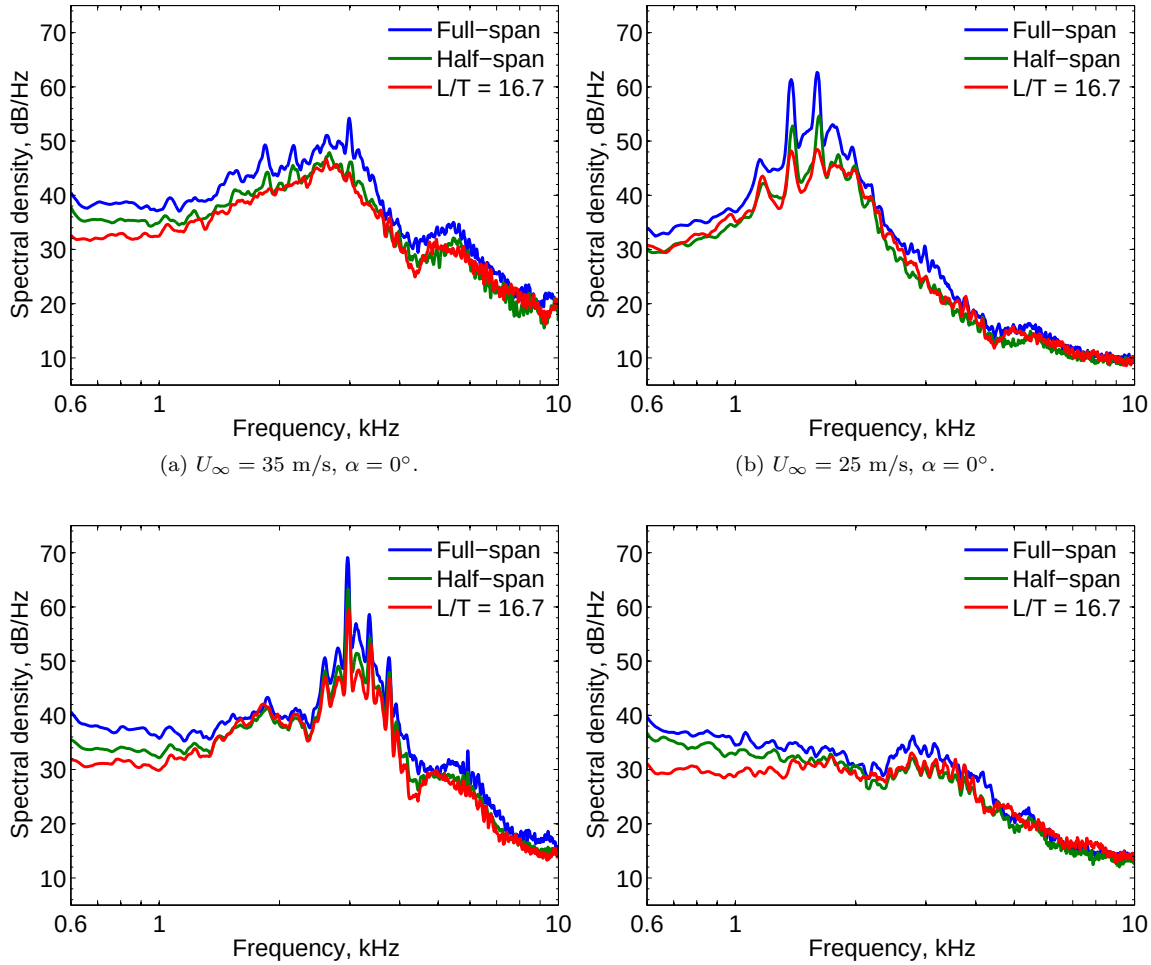

(a) $U_\infty = 35$ m/s, $\alpha = 0°$.

(b) $U_\infty = 25$ m/s, $\alpha = 0°$.

(c) $U_\infty = 35$ m/s, $\alpha = 1.6°$.

(d) $U_\infty = 35$ m/s, $\alpha = 3.2°$.

Figure 13: Far-field acoustic spectra for the wall-mounted finite airfoil with $L/T = 16.7$ compared to the full-span and half-span airfoil.

envelope the entire airfoil.

To examine the effect of angle of attack on noise source location, Fig. 16 shows sound maps taken with the top microphone array for the wall-mounted airfoil with $L/T = 16.7$ at a flow speed of $U_\infty = 35$ m/s and angles of attack of $\alpha = 1.6$ and 3.2°. At an angle of attack of $\alpha = 1.6°$, the wall-mounted finite airfoil behaves similarly to its zero angle of attack counterpart (see Fig. 14) at frequencies up to 5 kHz. At 1 kHz, the noise source is compact while at higher frequencies of 2 kHz and above, trailing edge noise is dominant. At frequencies between 2 and 5 kHz, the noise source is located close to the airfoil's free end region and extends from its midspan to tip as observed at zero angle of attack. At 7 kHz however, the noise source shifts closer to the airfoil-wall junction and extends from the airfoil's midspan to the wall region.

When the angle of attack is increased to 3.2°, Fig. 16 shows the dominant noise source is located near the airfoil-wall junction at all frequencies. Increasing the airfoil angle of attack therefore shifts the dominant noise source location from near the airfoil's free end to the region of the airfoil-wall junction. At frequencies of 2 and 3.5 kHz, trailing edge noise dominates and the noise source extends from the airfoil's midspan to the airfoil-wall junction. At a frequency of 5 kHz, the dominant noise source is located at the corner of the airfoil trailing edge and wall junction. Additionally, noise sources are observed at the corner of the airfoil leading edge and wall junction and the corner of the airfoil trailing edge and tip. At a higher frequency of 7 kHz, the dominant noise source is located only at the corner of the airfoil trailing edge and wall junction.

Figure 17 shows sound maps taken with the side array located parallel to the airfoil's tip surface, hence the sound map is a side view. The contraction outlet and airfoil profile are shown in these figures in white. While

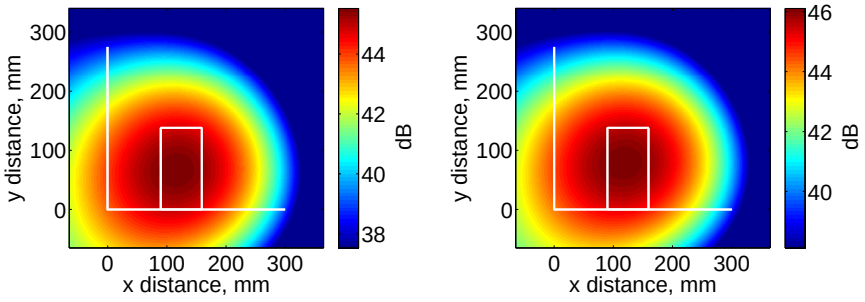

(a) $U_\infty = 35$ m/s, $f = 1$ kHz.

(b) $U_\infty = 25$ m/s, $f = 1$ kHz.

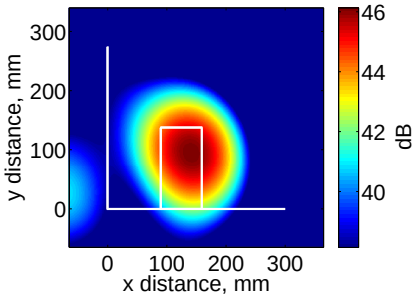

(c) $U_\infty = 35$ m/s, $f = 2$ kHz.

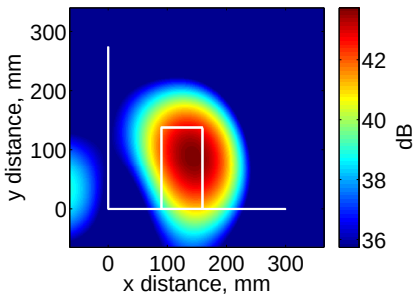

(d) $U_\infty = 25$ m/s, $f = 2$ kHz.

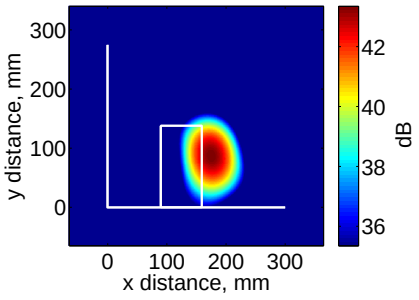

(e) $U_\infty = 35$ m/s, $f = 3.5$ kHz.

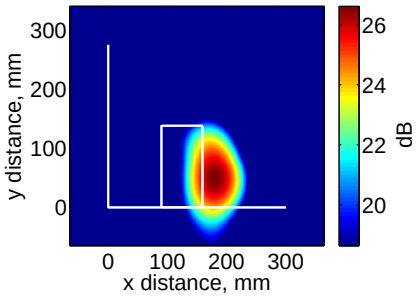

(f) $U_\infty = 25$ m/s, $f = 3.5$ kHz.

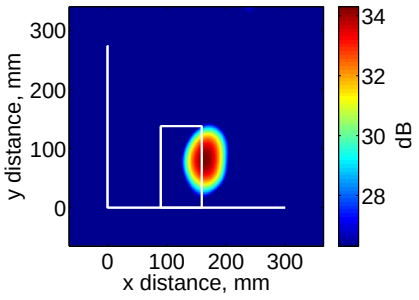

(g) $U_\infty = 35$ m/s, $f = 5$ kHz.

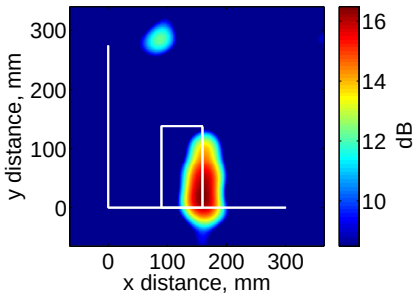

(h) $U_\infty = 25$ m/s, $f = 5$ kHz.

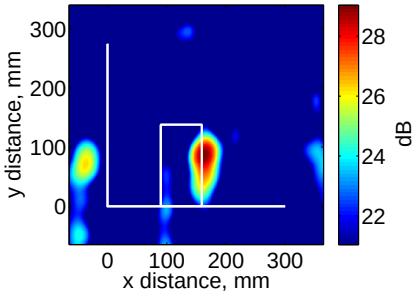

(i) $U_\infty = 35$ m/s, $f = 7$ kHz.

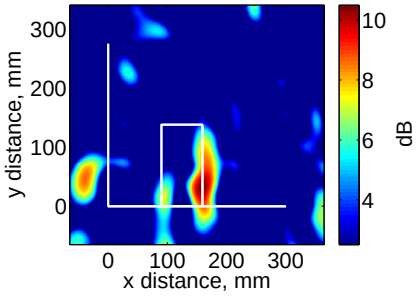

(j) $U_\infty = 25$ m/s, $f = 7$ kHz.

Figure 14: Sound maps taken with the top array for the wall-mounted finite airfoil with $L/T = 16.7$ at $U_\infty = 25$ and 35 m/s and zero angle of attack.

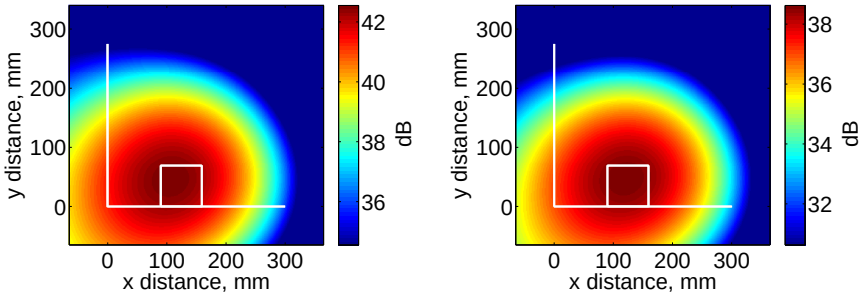

(a) $U_\infty = 35$ m/s, $f = 1$ kHz.

(b) $U_\infty = 25$ m/s, $f = 1$ kHz.

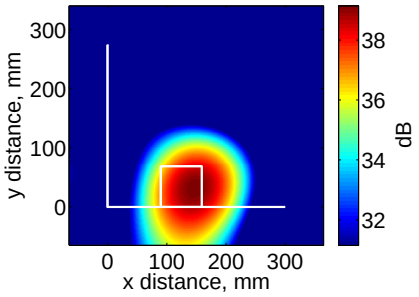

(c) $U_\infty = 35$ m/s, $f = 2$ kHz.

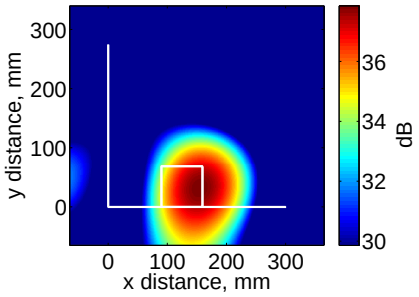

(d) $U_\infty = 25$ m/s, $f = 2$ kHz.

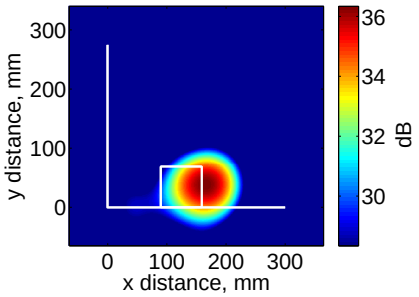

(e) $U_\infty = 35$ m/s, $f = 3.5$ kHz.

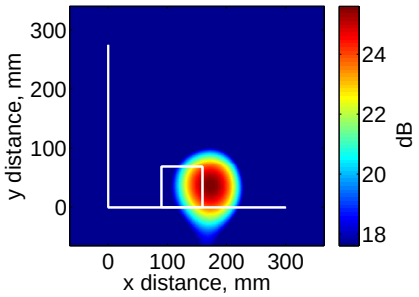

(f) $U_\infty = 25$ m/s, $f = 3.5$ kHz.

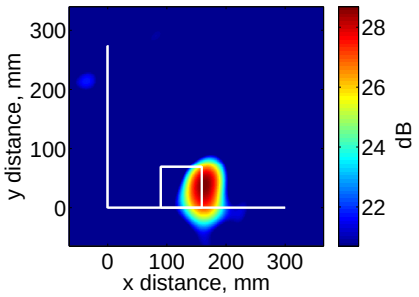

(g) $U_\infty = 35$ m/s, $f = 5$ kHz.

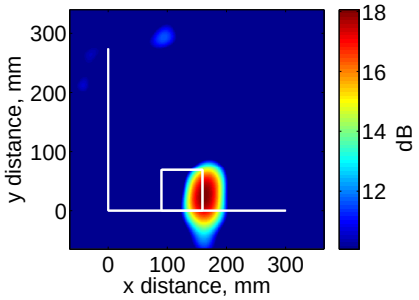

(h) $U_\infty = 25$ m/s, $f = 5$ kHz.

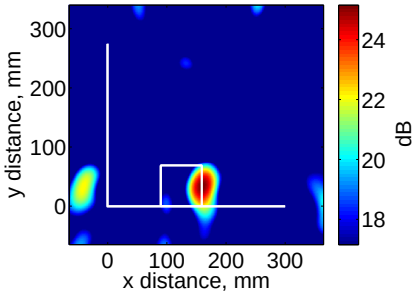

(i) $U_\infty = 35$ m/s, $f = 7$ kHz.

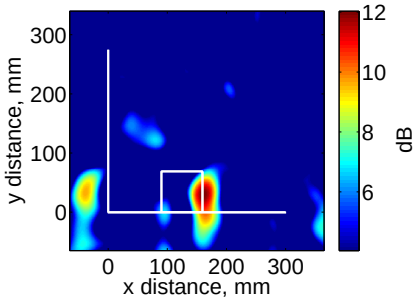

(j) $U_\infty = 25$ m/s, $f = 7$ kHz.

Figure 15: Sound maps taken with the top array for the wall-mounted finite airfoil with $L/T = 8.3$ at $U_\infty = 25$ and 35 m/s and zero angle of attack.

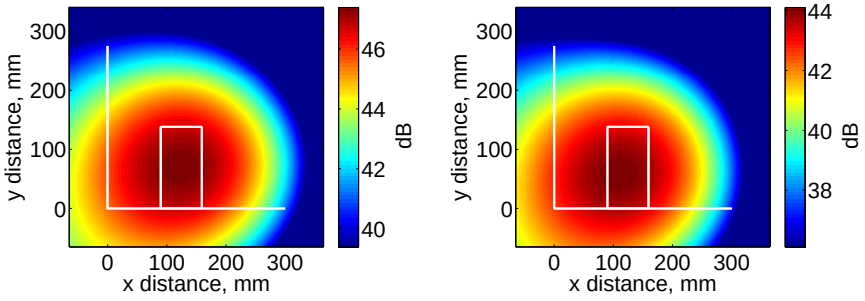

(a) $\alpha = 1.6°$, $f = 1$ kHz.

(b) $\alpha = 3.2°$, $f = 1$ kHz.

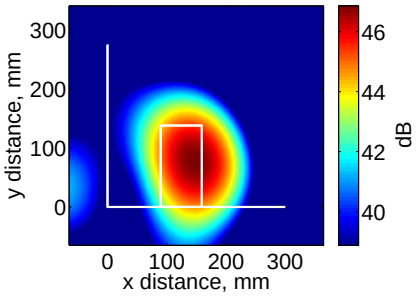

(c) $\alpha = 1.6°$, $f = 2$ kHz.

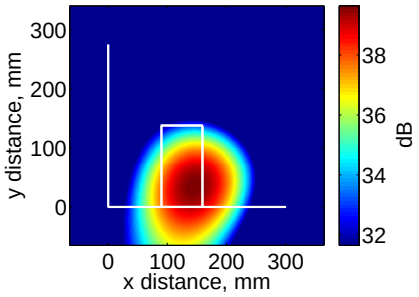

(d) $\alpha = 3.2°$, $f = 2$ kHz.

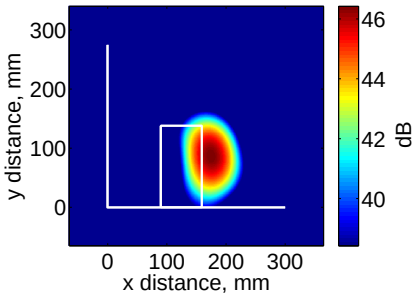

(e) $\alpha = 1.6°$, $f = 3.5$ kHz.

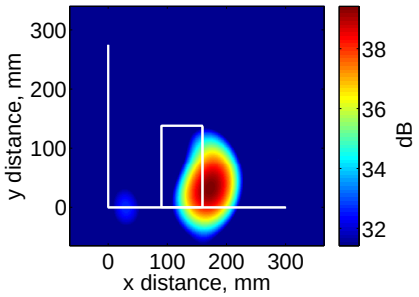

(f) $\alpha = 3.2°$, $f = 3.5$ kHz.

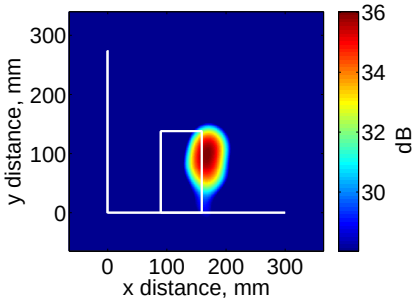

(g) $\alpha = 1.6°$, $f = 5$ kHz.

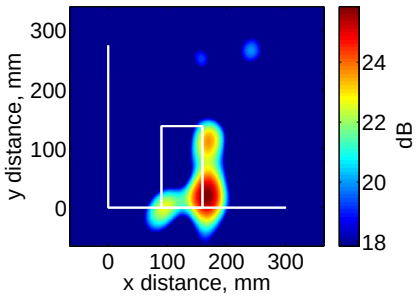

(h) $\alpha = 3.2°$, $f = 5$ kHz.

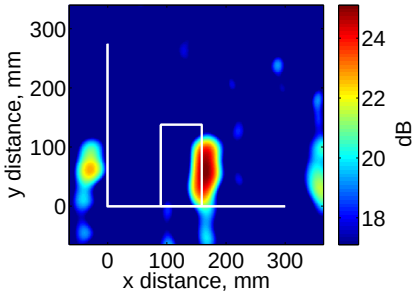

(i) $\alpha = 1.6°$, $f = 7$ kHz.

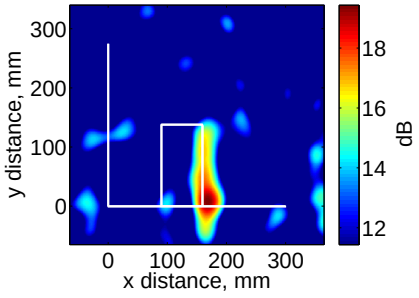

(j) $\alpha = 3.2°$, $f = 7$ kHz.

Figure 16: Sound maps taken with the top array for the wall-mounted finite airfoil with $L/T = 16.7$ at $U_\infty = 35$ m/s and non-zero angle of attack.

sound maps are presented at a frequency of 3.5 kHz and for $L/T = 16.7$ only, the results are characteristic of those occurring over the entire frequency range of interest and for all airfoil aspect ratios.

At all angles of attack ($\alpha = 0 - 3.2°$), the sound maps in Fig. 17 produced with monopolar beamforming show two strong equi-spaced lobes above and below the airfoil trailing edge. This indicates that the dominant noise source is trailing edge noise with dipolar directivity. The two equi-spaced lobes are observed to rotate slightly with airfoil angle of attack so that they are orientated normal to the airfoil surface. The dipole nature of the sound source is confirmed by examining the sound maps produced with dipolar beamforming which show the multiple lobes collapse to a single source at the airfoil trailing edge.

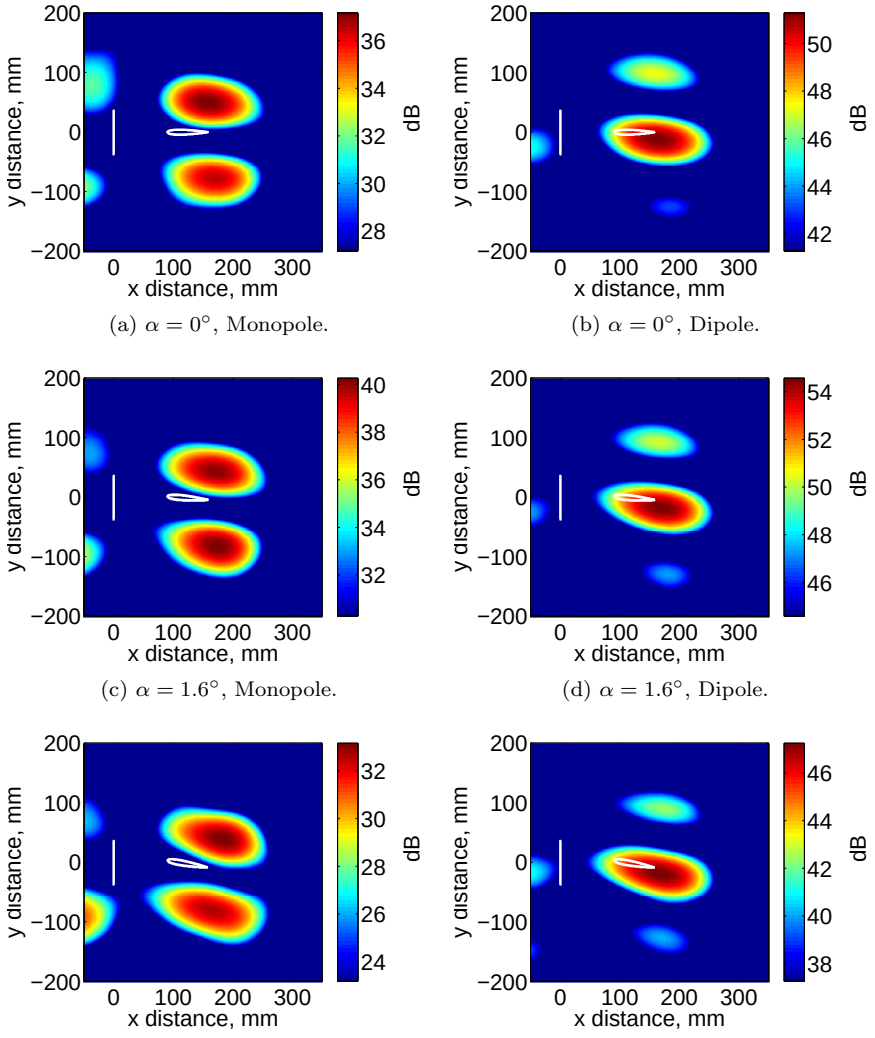

(a) $\alpha = 0°$, Monopole. (b) $\alpha = 0°$, Dipole.

(c) $\alpha = 1.6°$, Monopole. (d) $\alpha = 1.6°$, Dipole.

(e) $\alpha = 3.2°$, Monopole. (f) $\alpha = 3.2°$, Dipole.

Figure 17: Sound maps taken with the side array at $f = 3.5$ kHz for the wall-mounted finite airfoil with $L/T = 16.7$ at $U_\infty = 35$ m/s.

IV. Conclusion

This paper has presented results of an experimental investigation on the noise generated by a wall-mounted finite length airfoil at low-to-moderate Reynolds number. Far-field acoustic spectra and sound maps taken with two perpendicular planar microphone arrays have been presented for a wall-mounted finite airfoil with a variety of aspect ratios and at a range of Reynolds numbers and angles of attack. Flow speed has been shown to significantly effect the spectral content of sound radiated by the wall-mounted finite airfoil and to influence whether tonal noise production occurs as well as the magnitude and frequency of any tonal

noise components. Increasing the angle of attack increases the flow speed at which tones are produced by the wall-mounted finite airfoil with tonal noise production only occurring for a wall-mounted finite airfoil with aspect ratio of $L/T > 8.3$.

Acoustic beamforming results show that at zero angle of attack, trailing edge noise with dipole like directivity is the dominant noise generation mechanism of the wall-mounted finite airfoil at a frequency of 1 kHz and above. At high aspect ratio and flow speed, the trailing edge noise source is located near the airfoil tip. Increasing the airfoil angle of attack shifts the dominant noise source location from the airfoil tip to near the airfoil-wall junction. At an angle of attack of 3.2° trailing edge noise near the airfoil-wall junction dominates but additional noise sources are also observed at the corner of the airfoil leading edge and wall junction and the corner of the airfoil trailing edge and tip.

Acknowledgments

This work has been supported by the Australian Research Council under linkage grant LP110100033 'Understanding and predicting submarine hydrofoil noise'.

References

[1]T.F. Brooks, D. Pope and M. Marcolini, "Airfoil self noise and prediction", Technical report, NASA Reference Publication 1218, 1989.

[2]T.F. Brooks and T.H. Hodgson, "Trailing edge noise prediction from measured surface pressures", *Journal of Sound and Vibration* 78(1) (1981) 69 – 117.

[3]H. Arbey and J. Bataille, "Noise generated by airfoil profiles placed in a uniform laminar flow", *Journal of Fluid Mechanics* 134 (1983) 33 – 47.

[4]T.F. Brooks and M.A. Marcolini, "Scaling of airfoil self-noise using measured flow parameters", *AIAA Journal* 23(2) (1985) 207 – 213.

[5]W.K. Blake, *Mechanics of Flow Induced Sound and Vibration*, volume II: Complex flow-structure interactions, Academic Press, New York, 1986.

[6]M.S. Howe, *Hydrodynamics and Sound*, Cambridge University Press, New York, 2006.

[7]M. Herr, C. Appel, J. Dierke and R. Ewert, "Trailing-edge noise data quality assessment for CAA validation", *16th AIAA/CEAS Aeroacoustics Conference*, AIAA 2010 – 3877, Stockholm, Sweden, 2010.

[8]D.J. Moreau, L.A. Brooks and C.J. Doolan, "The effect of boundary layer type on trailing edge noise from sharp-edged flat plates at low-to-moderate Reynolds number", *Journal of Sound and Vibration* 331(17) (2012) 3976 – 3988.

[9]M. Fink, "Prediction of airfoil tone frequencies", *Journal of Aircraft* 12(2) (1975) 118 – 120.

[10]R.E. Longhouse, "Vortex shedding noise of low tip speed, axial flow fans", *Journal of Sound and Vibration* 53 (1977) 25 – 46.

[11]L. Jones, R. Sandberg and N. Sandham, "Stability and receptivity characteristics of a laminar separation bubble on an aerofoil", *Journal of Fluid Mechanics* 648 (2010) 257 – 296.

[12]W.R Wolf, J.L.F. Azevedo and S.K. Lele, "Effects of mean flow convection, quadrupole sources and vortex shedding on airfoil overall sound pressure level", *Journal of Sound and Vibration* 332(26) (2013) 6905 – 6912.

[13]T.F. Brooks and M.A. Marcolini, "Airfoil tip vortex formation noise", *AIAA Journal* 24(2) (1986) 246 – 252.

[14]J.M. Kendall, "Measurements of noise produced by flow past lifting surfaces", *16th Aerospace Sciences Meeting (AIAA)*, AIAA 78 – 239, Huntsville, AL, 1978.

[15]R. Mehta, "Effect of wing nose shape on the flow in a wing body junction", *Aeronautical Journal* 88 (1984) 456.

[16]W.J. Devenport and R.L. Simpson, "Time-dependent and time-averaged turbulence structure near the nose of a wing-body junction", *Journal of Fluid Mechanics* 210 (1990) 23 – 55.

[17]S.M. Olcmen and R.L. Simpson, "Some features of a turbulent wing-body junction vortical flow", *International Journal of Heat and Fluid Flow* 27 (2006) 980 – 993.

[18]M. Giuni and R.B. Green, "Vortex formation on squared and rounded tip", *Aerospace Science and Technology* 29 (2013) 191 – 199.

[19]R.L. Simpson, "Junction flows", *Annual Review of Fluid Mechanics* 33 (2001) 415 – 443.

[20]D.J. Moreau, L.A. Brooks and C.J. Doolan, "Broadband trailing edge noise from a sharp-edged strut", *Journal of the Acoustical Society of America* 129(5) (2011) 2820 – 2829.

[21]J.R. Underbrink, *Aeroacoustic Measurements*, Springer, Berlin, 2002.

[22]T. Cebeci and P. Bradshaw, *Momentum Transfer in Boundary Layers*, Hemisphere Publishing Corporation, Washington, 1977.

[23]R.W. Paterson, P.G. Vogt and M.R. Fink, "Vortex noise of isolated airfoils", *Journal of Aircraft* 10(5) (1973) 296 – 302.

[24]M.V. Lowson, S.P. Fiddes and E.C. Nash, "Laminar boundary layer aeroacoustic instabilities", *32nd Aerospace Sciences Meeting (AIAA)*, AIAA 94 – 0358, Reno, NV, 1994.